KfK 2697
Oktober 1978

The Pressure Drop of Spacer Grids in Rod Bundles of 12 Rods with Smooth and Roughened Surfaces

K. Rehme
Institut für Neutronenphysik und Reaktortechnik
Projekt Schneller Brüter

Kernforschungszentrum Karlsruhe

KERNFORSCHUNGSZENTRUM KARLSRUHE GMBH
ISSN 0303-4003

KERNFORSCHUNGSZENTRUM KARLSRUHE

Institut für Neutronenphysik und Reaktortechnik
Projekt Schneller Brüter

KfK 2697

The pressure drop of spacer grids in rod bundles of 12 rods with smooth and roughened surfaces

by

K. Rehme

Kernforschungszentrum Karlsruhe GmbH., Karlsruhe

Abstract

Experiments have been performed on the pressure drop of spacer grids in rod bundles of 12 rods. Both a smooth and a rough rod bundle was used in the experiments. The artificial roughness cut into the outer surface of the rods was chosen such as to meet the actual design of a gas cooled fast breeder reactor. The results of this investigation for a Reynolds number range between $Re=4 \cdot 10^3$ and $7 \cdot 10^4$ indicate that the pressure drop at the spacer grids is higher in a roughened rod bundle than in a smooth rod bundle.

Der Druckverlust an Abstandshaltergittern in Stabbündeln von 12 Stäben mit glatten und rauhen Oberflächen

Zusammenfassung

Der Druckverlust an Abstandshaltern in Stabbündeln mit 12 Stäben wurde experimentell untersucht. Ein glattes und ein rauhes Stabbündel wurden bei den Untersuchungen verwendet. Die künstliche Rauhigkeit, die in die Oberfläche der Stäbe eingedreht wurde, war so gewählt, daß sie dem Referenzentwurf des gasgekühlten Schnellen Brüters entsprach. Die Ergebnisse dieser Untersuchung für einen Reynoldszahlbereich von $Re=4 \cdot 10^3-7 \cdot 10^4$ zeigen, daß der Druckverlust am Abstandshalter in einem rauhen Stabbündel größer ist als in einem glatten Stabbündel.

1. Introduction

In gas cooled fast breeder reactors (GCFR) artificial roughness is used on the fuel element surfaces in order to improve the heat transfer performance. Computer codes for the calculation of a detailed distribution of mass flow and wall and fluid temperatures in rod bundles with roughened pins require experimental information on the pressure drop and the improvement of heat transfer due to the spacer grids as input data. Data for the improvement of the heat transfer are reported in the literature /1,2/, information of the pressure drop of spacer grids is available only for spacer grids in smooth rod bundles /3/. In the case of roughened rod bundles the only results available stem from one experimental investigation by Eaton /4/. In this investigation "it was observed that the grid loss coefficients in the rough bundle were typically to 10% higher than those of the smooth bundle, although the experimental uncertainty prevents any definte conclusion." The measurements by Eaton covered a range of Reynolds numbers between $7 \cdot 10^3$ and $4 \cdot 10^4$. For the design of the 12-rod bundle irradiation test in the Belgian Reactor BR2 /5/ more reliable pressure drop data for the spacer grids were required, also at higher Reynolds numbers ($Re = 7 \cdot 10^4$). Therefore, pressure drop measurements were performed.

2. Experimental Setup

Experiments were conducted in a water loop /3/, since water tests result in a higher accuracy of the measurements and the expansion losses for a compressible fluid can be taken into account additionally. The mass flow rate through the test section was measured by means of turbine flowmeters and a magnetic flowmeter, respectively; the pressure differences were determined by means of U-tube pressure gauges; the manometer fluids used were dichloro ethane, carbon

tetrachloride and mercury against water. The temperature of the water was measured by two mercury thermometers. The test section consisted of 12 tubes arranged in a triangular array in a shroud of a special profile (scalloped) schematically shown in Fig. 1. All dimensions of the test section were chosen such as to meet the actual design of a GCFR except the number of rods in the rod bundle. The tubes were arranged at a pitch of P = 11.1 mm. Two different rod bundles were used, one with smooth rods and another with rods roughened all the way. The diameter of the smooth tubes was D_S = 8 mm O.D.. The rough tubes roughened by cutting a trapezoidal shape (Fig. 2) in the outer surface /5/ had a volumetric diameter of D_{vol} = 7.86 mm. The volumetric diameter of the roughened tube is calculated as volumetrically averaged outer diameter of the roughened surface. Thus, the pitch-to-diameter ratios of the tubes were P/D_S = 1.39 for the smooth and P/D_{vol} = 1.41 for the rough bundle. The distance between the center of a tube adjacent to the shroud wall and the wall proper was 5.78 mm, resulting in a wall-to-diameter ratio of W/D_{vol} = 1.24. The length of the bundle was L = 900 mm. The tubes were supported by spacer grids at five levels over their entire length (Fig. 3). Fig. 4 shows one of the spacer grids used (SI), a honeycombtype grid fabricated by spark erosion. Small ceramic strips guided in the grid structure were used as stand-offs, since those grids had been used for heat transfer tests /5/ and the ceramic strips were necessary for electrical insulation of the directly heated tubes. The axial length of the spacer grids was h = 14 mm. Four different spacer grids were tested:

SI: original design

SII: same as SI but leading edges of the grids sharpened

SIIIS: new design, with reduced blockage near the shroud

SIIIR: same as SIIIS. but with leading edges rounded (Fig. 5).

The blockage factors of the grids

$$\varepsilon = \frac{A_{sp}}{A} \qquad (1)$$

that is, projected area of the spacer including the ceramic strips divided by the flow area of the bundle away from the spacer, are listed in the table below.

spacer grid	SI; SII		SIIIS; SIIIR	
rod bundle	smooth	rough	smooth	rough
central subchannel	0.330	0.320	0.330	0.320
wall subchannel	0.383	0.372	0.204	0.199
corner subchannel without standoff	0.125	0.122	0.125	0.122
with standoff	0.491	0.478	0.491	0.478
total	0.348	0.338	0.280	0.271

Blockage factors of spacer grids /6/

3. Results and Discussion

The experiments were performed for a range of Reynolds number between $Re = 4 \cdot 10^3$ and $Re = 7 \cdot 10^4$. The Reynolds number is defined as

$$Re = \frac{\rho \, U_m \, D_h}{\mu} \qquad (2)$$

with ρ as the density of the fluid, U_m the velocity averaged across the flow area, D_h the hydraulic diameter of the bundle with a wetted perimeter including the shroud wall, and μ as the fluid viscosity. The pressure losses Δp were determined over a length of

ΔL_{sp} = 199.7 mm (A-B) including one spacer grid, and over a length of ΔL = 127.6 mm (C-B) and ΔL = 113.0 mm, respectively, between two spacer grids. The pressure drop over the length of ΔL = 127.6 was not influenced by the spacer grids, as initial detailed pressure drop measurements between two grids had shown: the pressure gradient between the pressure taps D and B was constant.
The pressure drop without a spacer grid is defined by

$$\frac{\Delta P}{\Delta L} = \lambda \frac{\rho}{2} U_m^2 \frac{1}{D_h} \qquad (3)$$

with λ as the Darcy friction factor. In the case of one spacer included in the length on which the pressure drop is measured we get

$$\Delta P = \left(\frac{\lambda \cdot \Delta L_{sp}}{D_h} + \zeta\right) \frac{\rho}{2} U_m^2 = \lambda' \frac{\rho}{2} U_m^2 \frac{\Delta L_{sp}}{D_h}. \qquad (4)$$

Thus, according to Eqs. (3) and (4), the drag coefficient of the spacer is calculated as

$$\zeta = (\lambda' - \lambda) \frac{\Delta L_{sp}}{D_h}. \qquad (5)$$

Assuming that the pressure drop at the spacer is mainly a drag loss due to the blockage of the flow cross section in the spacer region as earlier measurements indicated /3/ a modified loss coefficient C_v is defined as

$$\zeta = C_v \varepsilon^2. \qquad (6)$$

This modified loss coefficient is used in the SAGAPO code /7/ for the thermo- and fluiddynamic calculations of roughened rod bundles.

Fig. 6 shows the friction factors (SI) measured without spacer grids (λ) and including one spacer grid (λ') for both the smooth and the rough tube bundles as a function of the Reynolds number. The friction factors for the smooth bundle are 5% to 17% higher than

the values for smooth circular tubes. The difference between the measured friction factors and the circular tube values increases with the Reynolds number. A theoretical prediction of the friction factor for the smooth bundle results in a value coincident with the circular tube correlation /8/. Therefore, these higher friction factors are attributed to a certain roughness of the shroud wall, which is indicated by the slightly lower dependence of the friction factors measured on the Reynolds number than for smooth tubes.

The friction factors for the rough bundle at low Reynolds number increase with the Reynolds number, indicating a transitional behavior of the roughness effect on the flow, i.e. the transition from a hydraulic smooth to a fully rough condition. At higher Reynolds numbers ($Re \sim 3 \cdot 10^4$), the friction factors of the rough bundle become approximately constant and at even higher Reynolds numbers (the roughness behaviour now in a fully rough condition) the friction factors slightly decrease with the Reynolds number due to the effect of the smooth shroud wall on the pressure drop, since the friction factor at the shroud wall decreases with higher Reynolds numbers.

The drag coefficients ζ and the modified loss coefficients C_v of the spacer SI are plotted vs. the Reynolds number in Fig. 7. Both coefficients decrease with increasing Reynolds numbers. There is a considerable difference between the values in a smooth rod bundle and those in a rough rod bundle, the values for the rough bundle being higher. This difference amounts to drag coefficients of the spacer 26% higher in a rough bundle at a Reynolds number of $Re=7 \cdot 10^4$ and 19% at $Re = 10^4$. Due to the different blockage factors of the spacer grid in the rough and the smooth bundles, the modified drag coefficients are 34% higher in the rough bundle at $Re = 7 \cdot 10^4$ and 26% at $Re = 10^4$. These rather large differences may be explained by the higher friction on the rough walls in the spacer region than in the smooth bundle.

Similar results were obtained for the other spacers (SII,SIIIS, SIIIR). It is surprising that the spacer SII (Fig.8) shows higher

friction factors than the spacer SI although the spacer SII had sharpened leading edges by which the pressure drop was expected to be reduced. An inspection of the leading edges showed that the sharpening had led to burrs by which the blockage was increased, therefore, resulting in a higher pressure drop.

The spacers SIIIS (Fig.10) and SIIIR (Fig.12) had remarkably reduced friction factors compared with the spacers SI and SII. This is due to their lower overall blockage. A comparison of the friction factors with spacer grids between the spacer SIIIS (sharp leading edge) and SIIIR (rounded leading edge) shows that the pressure drop performance of the spacer was improved substantially by rounding the leading edge for a smooth rod bundle, whereas for the roughened bundle the friction factor approximately remained constant.

The drag coefficients of all spacers calculated by Eq. (5) are plotted in Fig. 14 for the smooth rod bundle and in Fig. 15 for the roughened rod bundle versus the Reynolds number. The figures clearly demonstrate the improvement achieved. The first modification (SI→SII) by sharpening the leading edges turned out to be a step in the wrong direction.

For the smooth bundle the drag coefficient was increased by 16% at $Re = 7 \cdot 10^4$ using the drag coefficient of SI as a reference. By reducing the blockage of the spacer the drag coefficient was reduced to 0.76 and by rounding the leading edge to 0.6.

For the roughened rod bundle the sharpening of the leading edges of SI (SII) resulted in an increase of the drag coefficient of 6.5%. By reducing the blockage of the spacer the drag coefficient was reduced to 0.68; this reduction is higher than for a smooth rod bundle. The rounding of the leading edge reduced the drag coefficient to 0.62.

It is very interesting to note that the rounding of the leading edges of the spacer reduces the drag coefficient of the spacer more (26%) in a smooth rod bundle than in a roughened rod bundle (9%).

4. Conclusions

The experimental investigation on the pressure drop of spacer grids in a rod bundle of 12 rods showed how the pressure drop performance of the grids was improved step by step.
Since, in the 12-rod bundle investigated, the portion of the smooth shroud walls is rather high compared with the actual GCFR fuel element design of 271 pins /9/, even higher drag coefficients compared to the results of this investigation are to be expected in this case. Also a different axial length of the spacer grid will have an influence on the pressure loss at the grid since the friction pressure drop in the spacer region will increase with an increasing axial length of the spacer grid. To establish reliable correlations for the pressure drop at the spacer grids in the GCFR reference design further experimental investigations are necessary.

Acknowledgments

The author would like to express his gratitude to Messrs. J. Marek and G. Wörner for their cooperation in performing the experiments.

References

/1/ M. Hudina and H. Nöthiger
Experimental study of local heat transfer under and near grid spacers developed for GCFR
(1973) unpublished

/2/ J. Marek and K. Rehme
Experimental investigation on the temperature distribution near spacer grids
Report KFK 2108, Nuclear Research Center Karlsruhe (1975) (in German)

/3/ K. Rehme
Pressure drop correlations for fuel element spacers
Nucl. Technology 17, 15-23 (1973)

/4/ T.E. Eaton
Gas-cooled fast reactor fuel element thermal-hydraulic investigations
D.Sc. Thesis, MIT (1975)

/5/ M. Dalle Donne, J. Marek, A. Martelli, K. Rehme
BR2 bundle mockup heat transfer experiments
Nucl. Engng. Design 40, 143-156 (1977)

/6/ W. Jung
Drag coefficients of spacer grid of HELM-calibration bundles
(unpublished) (in German)

/7/ A. Martelli
SAGAPO, a code for the prediction of steady state heat transfer and pressure drops in gas cooled bundles of rough and smooth rods
3rd NEA-GCFR Heat Transfer Specialist Meeting, Petten (1975)

/8/ K. Rehme
Simple method of predicting friction factors of turbulent flow in non-circular channels
Int. J. Heat Mass Transfer 16, 933-950 (1973)

/9/ P. Rau
Concept of the fuel element of a 1000 MWe GCFR
Reaktortagung, Nürnberg 1975, p. 463 (1975) (in German)

Nomenclature

A	flow area; m^2
C_v	modified loss coefficient; -
D	diameter; m
D_h	equivalent diameter; m
L	length; m
P	pitch of the tubes; m
ΔP	pressure loss; Nm^{-2}
Re	Reynolds number; -
U	fluid velocity; ms^{-1}
W	wall distance (pin diameter + minimum distance between tube and shroud); m
ε	blockage factor; -
λ	friction factor; -
μ	viscosity; Kg $m^{-1}s^{-1}$
ρ	density; Kg m^{-3}
ζ	drag coefficient; -

Subscripts

m	mean
vol	volumetric; averaged over the roughened surface
R	rough
S	smooth
sp	spacer

Typ	SI		SI		SI		SI	
Spacer	without				without			
D_h [mm]	6.2218		6.2218		6.4865		6.4865	
ΔL [mm]	113.0		119.7		127.6		119.7	
ϵ	-		0.348		-		0.338	
Rod bundle	smooth		smooth		rough		rough	
	Re	λ	Re	λ'	Re	λ	Re	λ'
	$4.041 \cdot 10^3$	0.04508	$4.245 \cdot 10^3$	0.09832	$4.797 \cdot 10^3$	0.06233	$4.455 \cdot 10^3$	0.1262
	6.758	0.03624	7.290	0.07992	7.223	0.06257	7.274	0.1151
	$1.223 \cdot 10^4$	0.03190	$1.325 \cdot 10^4$	0.06809	$1.313 \cdot 10^4$	0.06504	$1.293 \cdot 10^4$	0.1140
	2.156	0.02854	2.316	0.06259	2.291	0.06892	2.388	0.1132
	3.207	0.02631	3.567	0.05751	3.413	0.06857	3.479	0.1106
	5.232	0.02374	5.457	0.05423	5.500	0.06686	5.431	0.1078
	6.503	0.02300	6.981	0.05258	6.204	0.06599	6.254	0.1059

Table 1: Pressure drop with and without spacer grid

Typ	SII		SII		SII		SII	
Spacer	without				without			
D_h [mm]	6.2218		6.2218		6.4865		6.4865	
ΔL [mm]	127.6		199.7		127.6		199.7	
ε	-		0.348		-		0.338	
Rod bundle	smooth		smooth		rough		rough	
	Re	λ	Re	λ'	Re	λ	Re	λ'
	$4.729 \cdot 10^3$	0.04292	$4.053 \cdot 10^3$	0.1013	$4.426 \cdot 10^3$	0.06024	$4.440 \cdot 10^3$	0.1211
	7.465	0.03547	7.141	0.08618	7.278	0.06153	7.263	0.1167
	$1.315 \cdot 10^4$	0.03161	$1.323 \cdot 10^4$	0.07301	$1.381 \cdot 10^4$	0.07179	$1.311 \cdot 10^4$	0.1161
	2.386	0.02455	2.362	0.06563	2.375	0.06735	2.342	0.1168
	3.627	0.02586	3.556	0.06131	3.473	0.06744	3.433	0.1144
	5.631	0.02392	5.603	0.05801	5.586	0.06772	5.602	0.1112
	7.060	0.02280	6.870	0.05665	6.143	0.06691	6.143	0.1104

Table 1 cont.

Typ	SIII		SIII		SIII		SIII	
Spacer	without				without			
D_h [mm]	6.2218		6.2218		6.4865		6.4865	
ΔL [mm]	113.0		199.7		127.6		199.7	
ε	-		0.28		-		0.271	
Rod bundle	smooth		smooth		rough		rough	
	Re	λ	Re	λ'	Re	λ	Re	λ'
S	$4.755 \cdot 10^3$	0.04333	$4.586 \cdot 10^3$	0.08315	$4.855 \cdot 10^3$	0.06515	$4.473 \cdot 10^3$	0.1021
	7.947	0.03434	7.843	0.06860	7.766	0.06365	7.566	0.09576
	$1.422 \cdot 10^4$	0.03104	$1.421 \cdot 10^4$	0.05911	$1.365 \cdot 10^4$	0.06714	$1.385 \cdot 10^4$	0.09544
	2.523	0.02850	2.516	0.05432	2.434	0.07085	2.437	0.09681
	3.873	0.02604	3.843	0.05130	3.609	0.07045	3.532	0.09526
	5.989	0.02309	6.043	0.04659	6.055	0.06604	6.120	0.08616
	7.781	0.02143	7.743	0.04273	6.569	0.06789	6.520	0.08688
R	$4.041 \cdot 10^3$	0.04508	$4.846 \cdot 10^3$	0.07256	$4.797 \cdot 10^3$	0.06233	$4.502 \cdot 10^3$	0.09997
	6.758	0.03624	7.017	0.06404	7.223	0.06257	7.295	0.09411
	$1.223 \cdot 10^4$	0.03190	$1.308 \cdot 10^4$	0.05430	$1.313 \cdot 10^4$	0.06504	$1.276 \cdot 10^4$	0.09173
	2.156	0.02854	2.304	0.04880	2.291	0.06892	2.284	0.09538
	3.207	0.02631	3.249	0.04629	3.413	0.06857	5.625	0.09425
	5.232	0.02374	5.273	0.04283	5.500	0.06686	5.625	0.09067
	6.503	0.02300	6.931	0.04087	6.204	0.06599	6.244	0.08972

Table 1 cont.

	Typ	SI		SII		SIIIS		SIIIG	
	Re	ζ	C_v	ζ	C_v	ζ	C_v	ζ	C_v
smooth rod bundel	$4 \cdot 10^3$	1.797	14.84	1.842	15.21			1.107	14.12
	5	1.618	13.36	1.704	14.07			0.985	12.57
	6	1.499	12.38	1.621	13.38	1.168	14.90	0.921	11.75
	8	1.374	11.35	1.486	12.27	1.066	13.59	0.841	10.73
	$1 \cdot 10^4$	1.297	10.71	1.403	11.58	1.011	12.90	0.790	10.07
	1.5	1.197	9.89			0.934	11.91	0.725	9.25
	2	1.133	9.36	1.242	10.26	0.889	11.34	0.690	8.80
	3	1.053	8.69	1.181	9.75	0.831	10.60	0.648	8.27
	4	1.011	8.35	1.149	9.49	0.793	10.11	0.623	7.94
	5	0.989	8.16	1.127	9.30	0.767	9.79	0.603	7.70
	6	0.969	8.00	1.114	9.20	0.741	9.46	0.587	7.49
	8	0.956	7.90	1.098	9.06	0.706	9.01	0.565	7.20
rough rod bundle	$4 \cdot 10^3$	2.01	17.60			1.318	17.81	1.272	17.19
	5	1.835	16.06			1.158	15.65	1.081	14.61
	6	1.724	15.09	1.786	15.63	1.124	15.19	0.998	13.48
	8	1.610	14.09	1.684	14.74	1.010	13.65	0.908	12.28
	$1 \cdot 10^4$	1.549	13.56	1.589	13.91	0.964	13.02	0.871	11.78
	1.5	1.465	12.83					0.831	11.24
	2	1.398	12.23	1.416	12.40	0.881	11.90	0.822	11.11
	3	1.318	11.53	1.376	12.05	0.868	11.73	0.801	10.82
	4	1.281	11.21	1.333	11.67	0.859	11.61	0.782	10.57
	5	1.247	10.91	1.318	11.53	0.840	11.36	0.760	10.28
	6	1.231	10.78	1.302	11.40	0.810	10.94	0.766	10.36
	8	1.201	10.51	1.287	11.26				

Table 2 Pressure drop coefficients of spacer grids

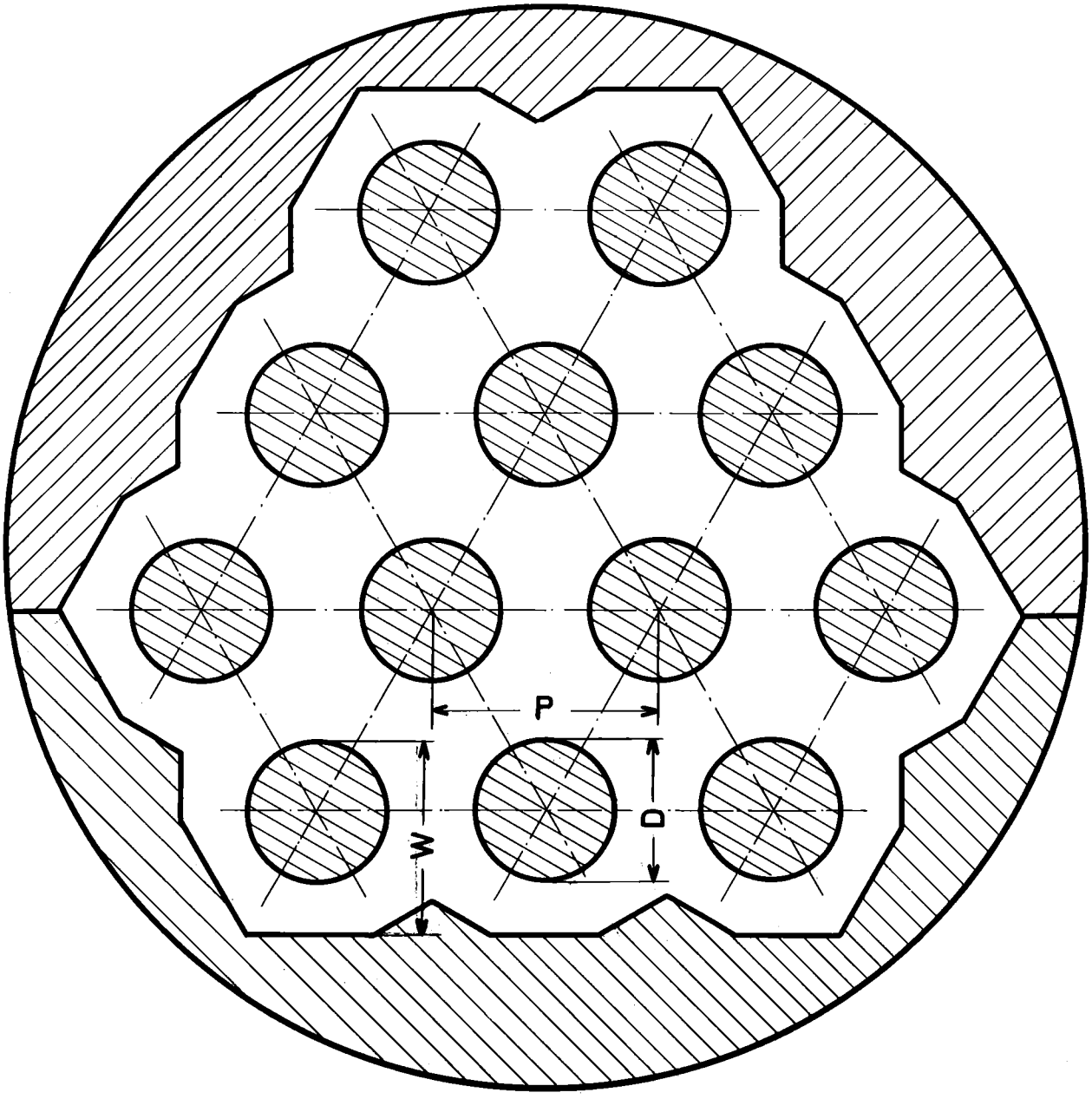

Fig. 1: Cross section of the rod bundle

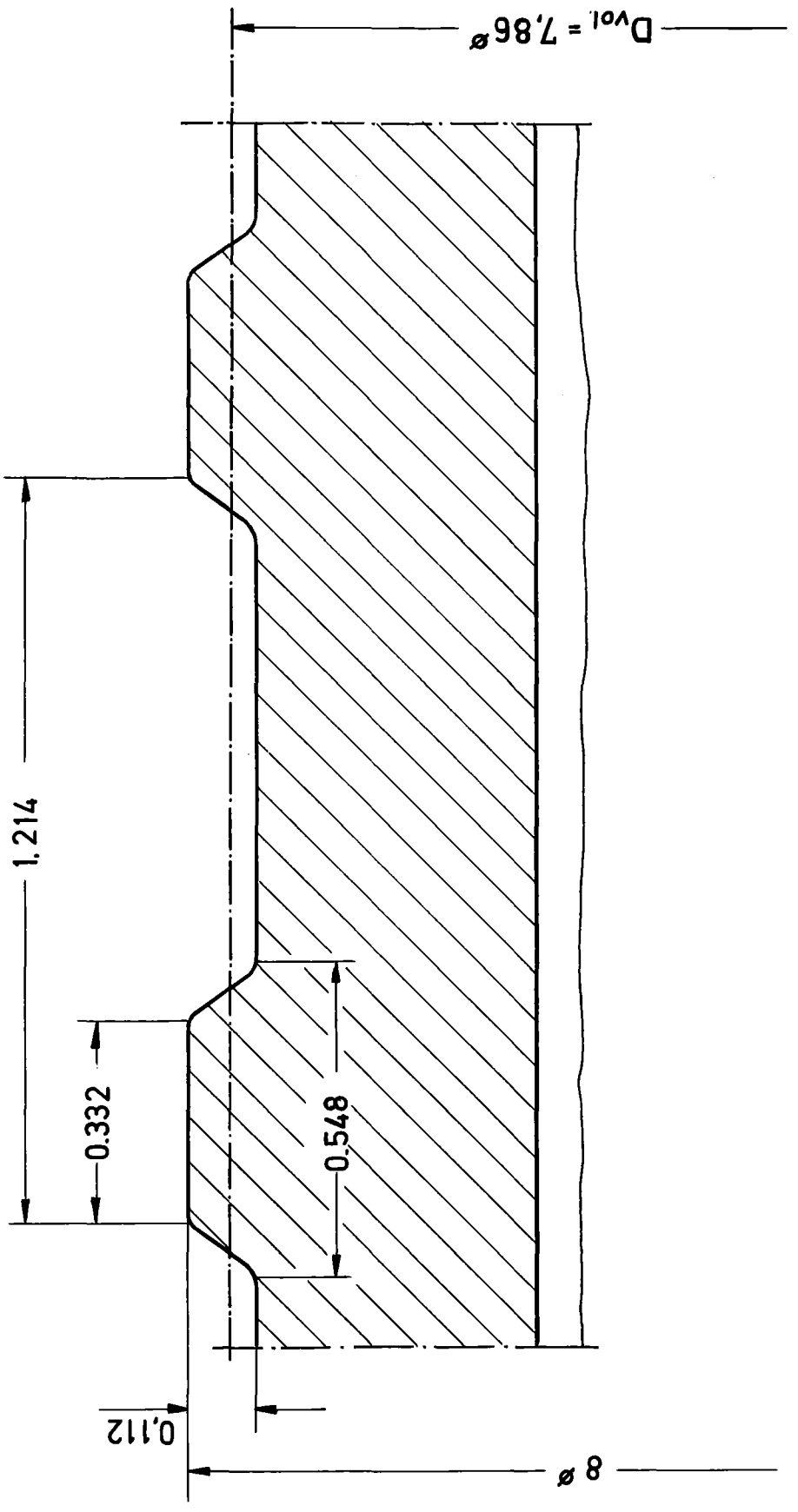

Fig. 2: Roughness profile (dimensions in mm)

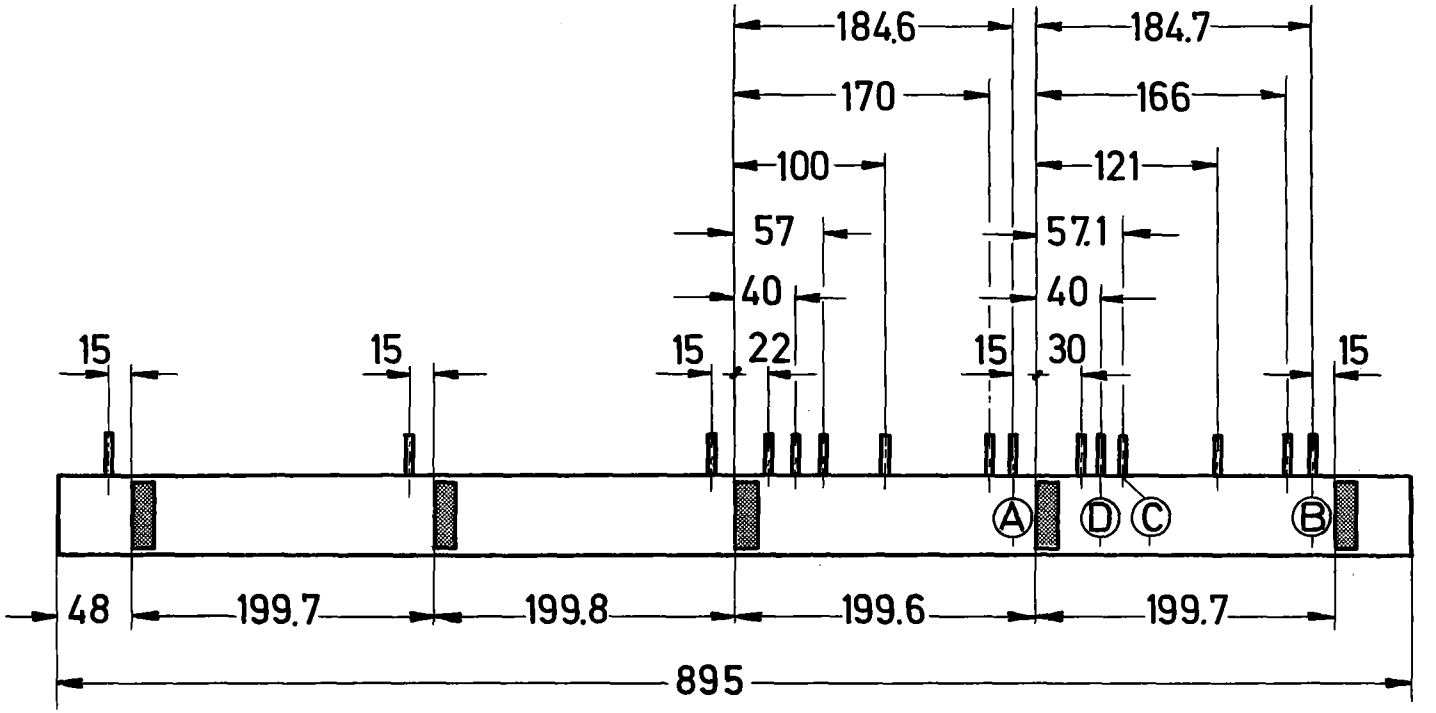

Fig. 3: Sketch of the axial geometry and positions of pressure taps (dimensions in mm)

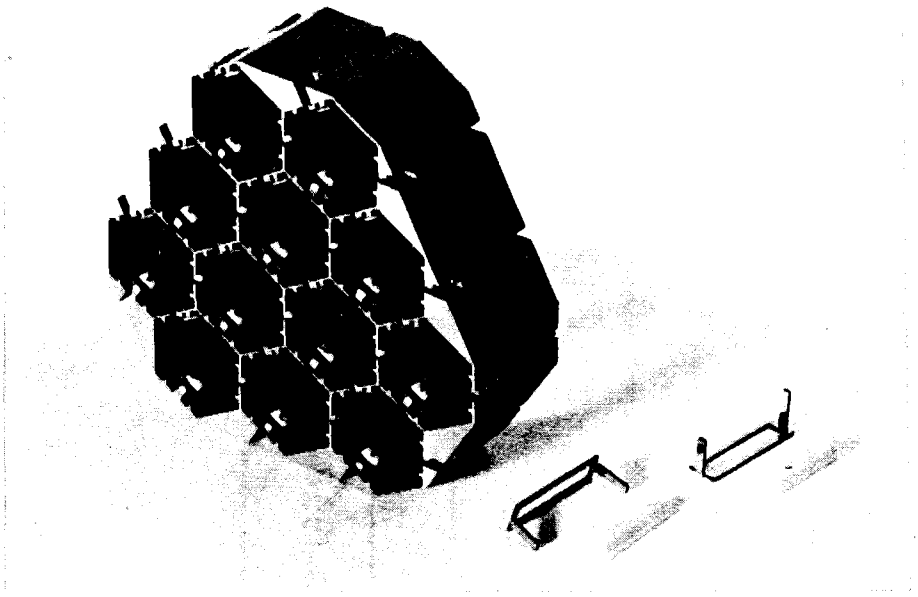

Fig. 4: Spacer grid (SI)

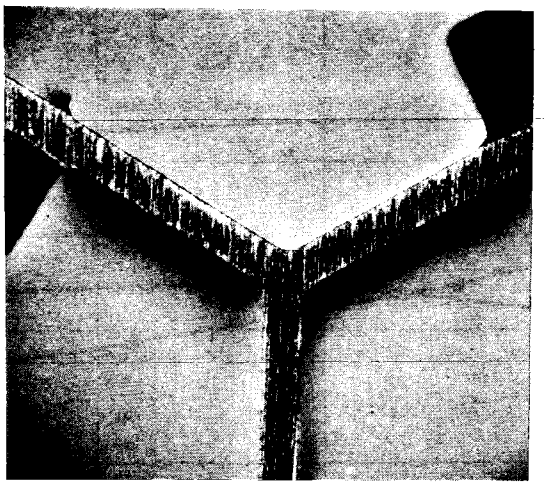

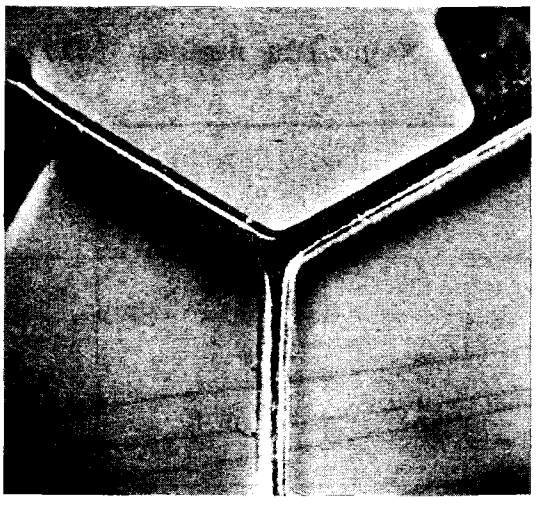

Fig. 5: Detail of spacer grid (SIIIS, SIIIR)

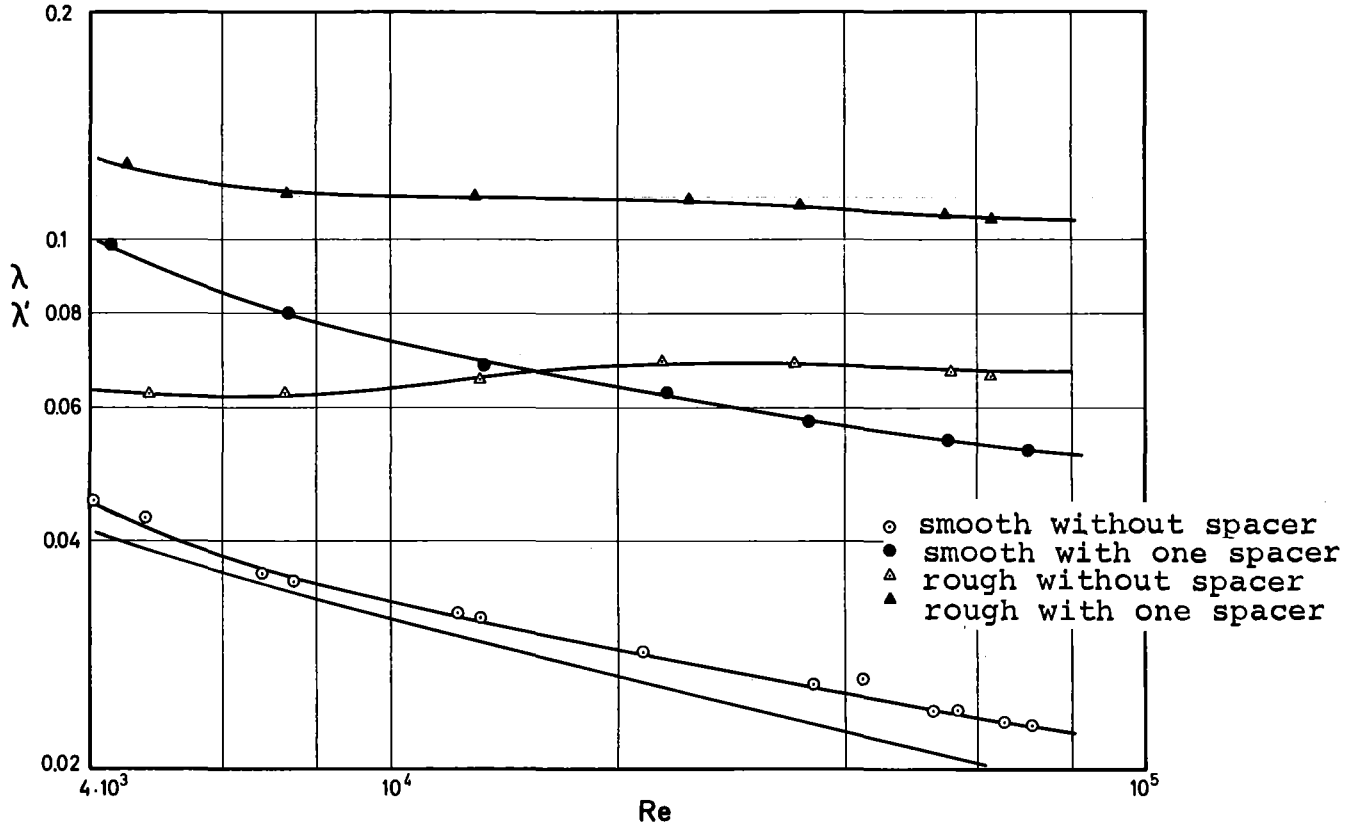

Fig. 6: Friction factors measured with and without spacer as a function of the Reynolds number (SI)

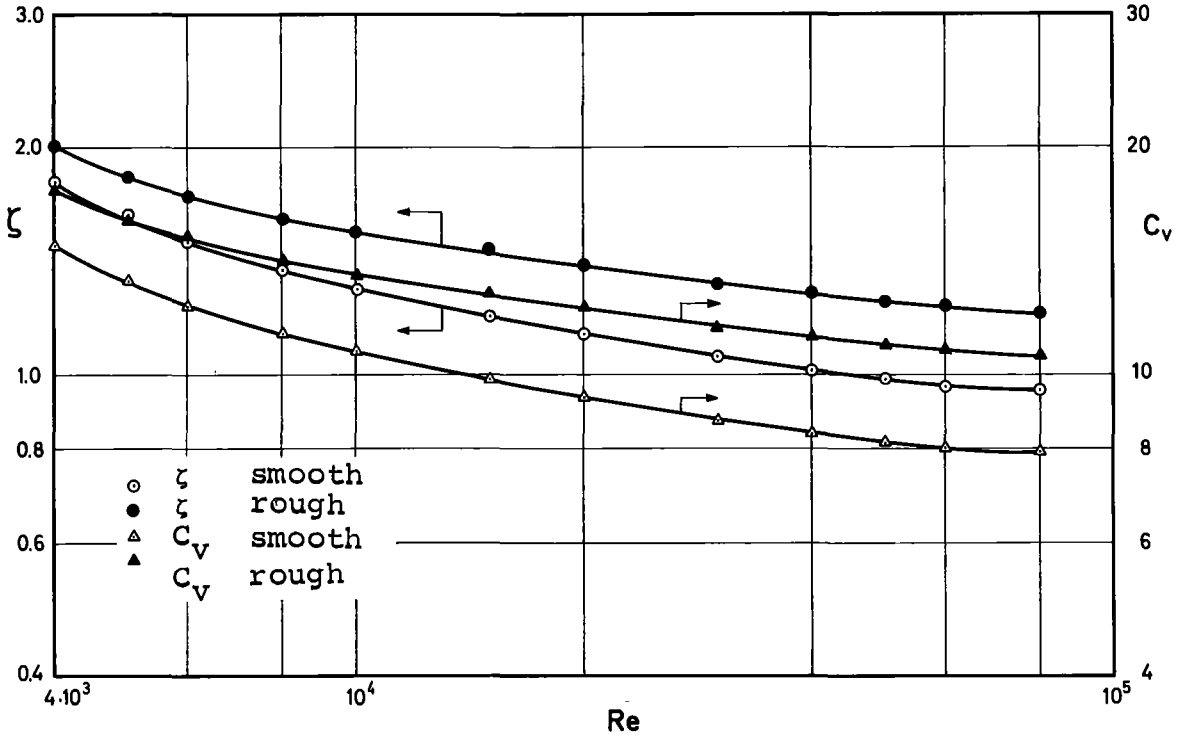

Fig. 7: Drag coefficients and modified loss coefficients versus Reynolds number (SI)

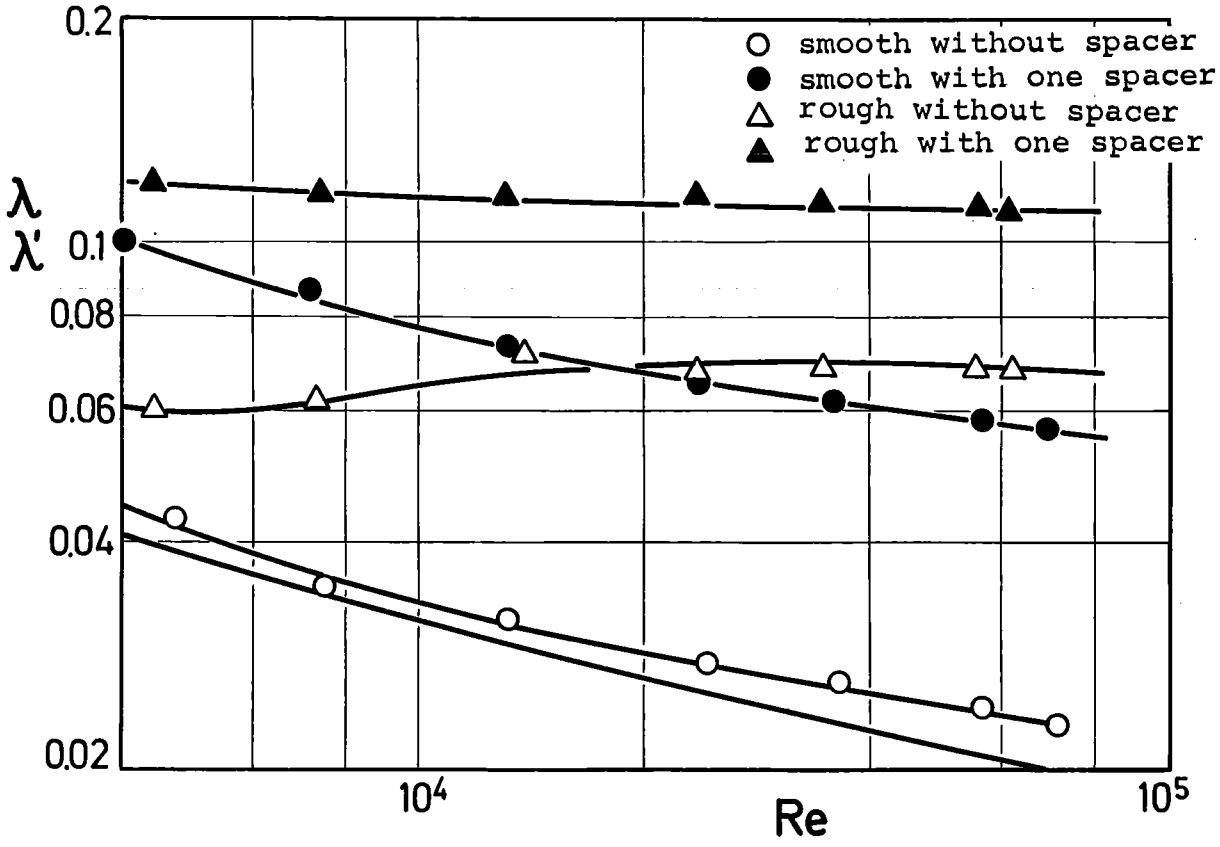

Fig. 8: Friction factors measured with and without spacer as a function of the Reynolds number (SII)

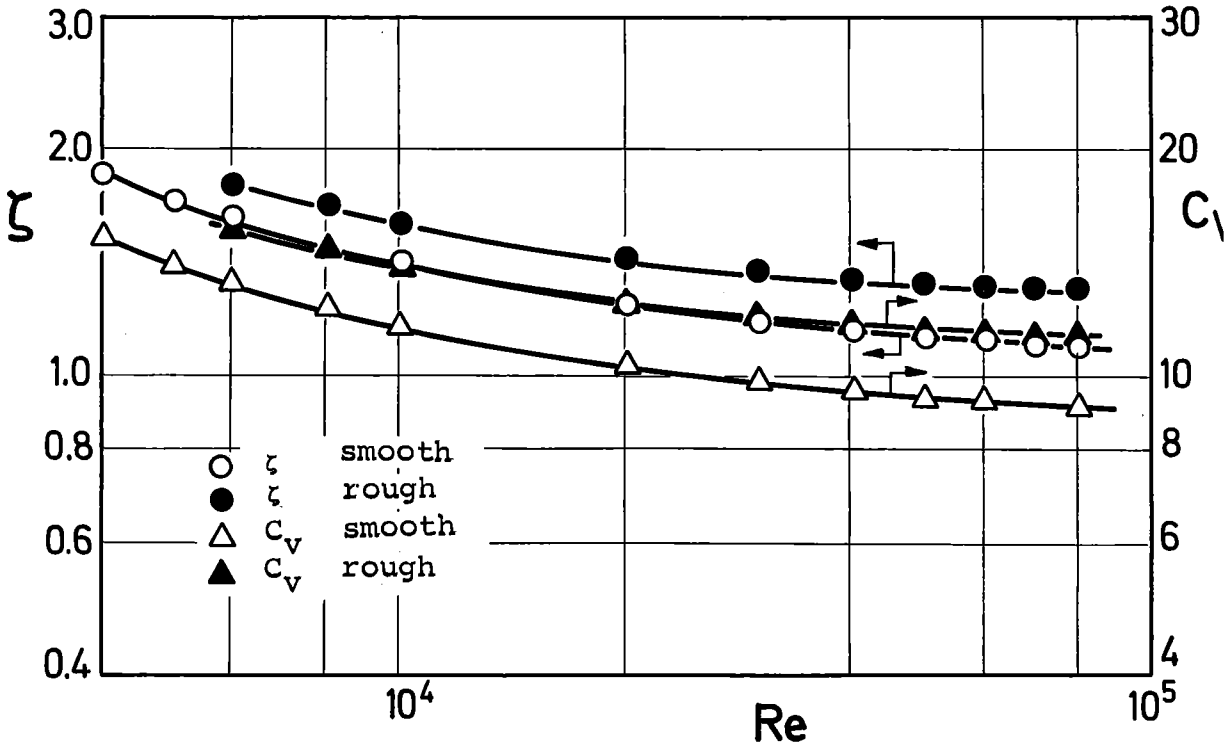

Fig. 9: Drag coefficients and modified loss coefficients versus Reanolds number (SII)

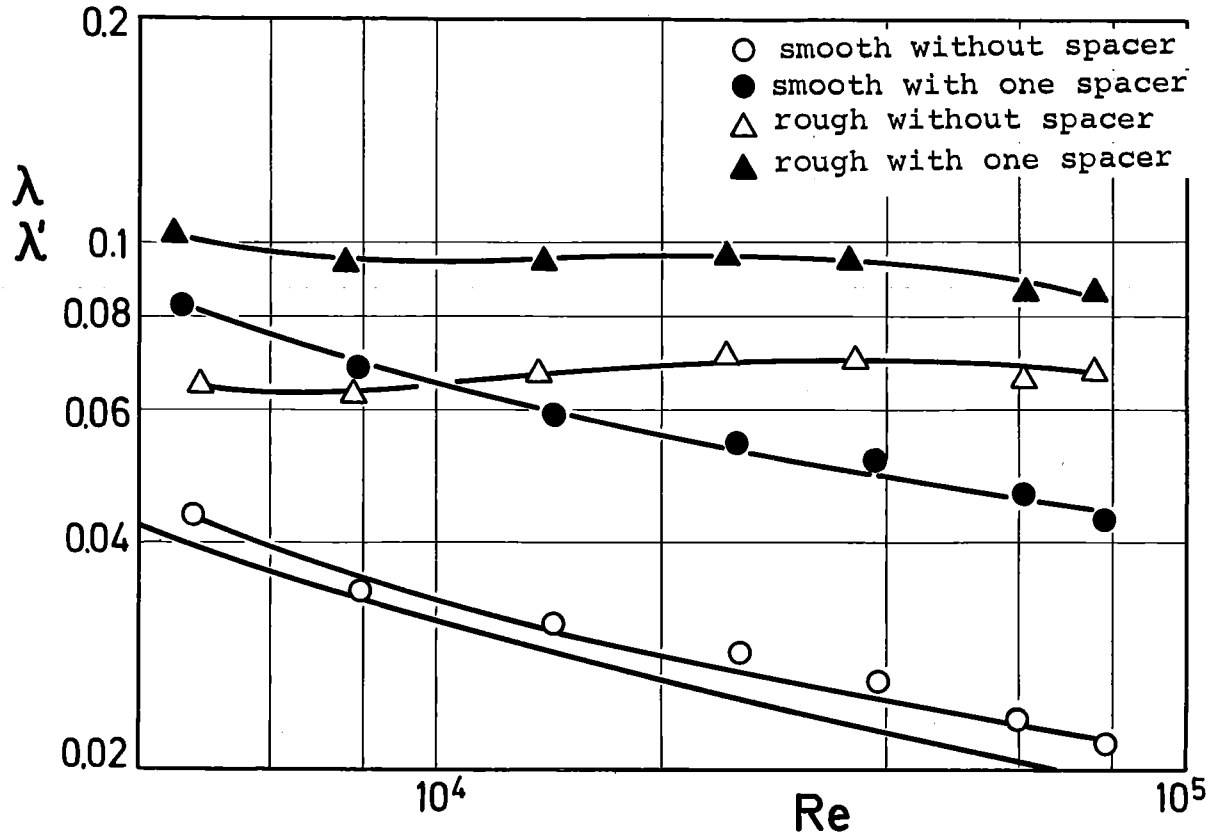

Fig.10: Friction factors measured with and without spacer as a function of the Reynolds number (SIIIS)

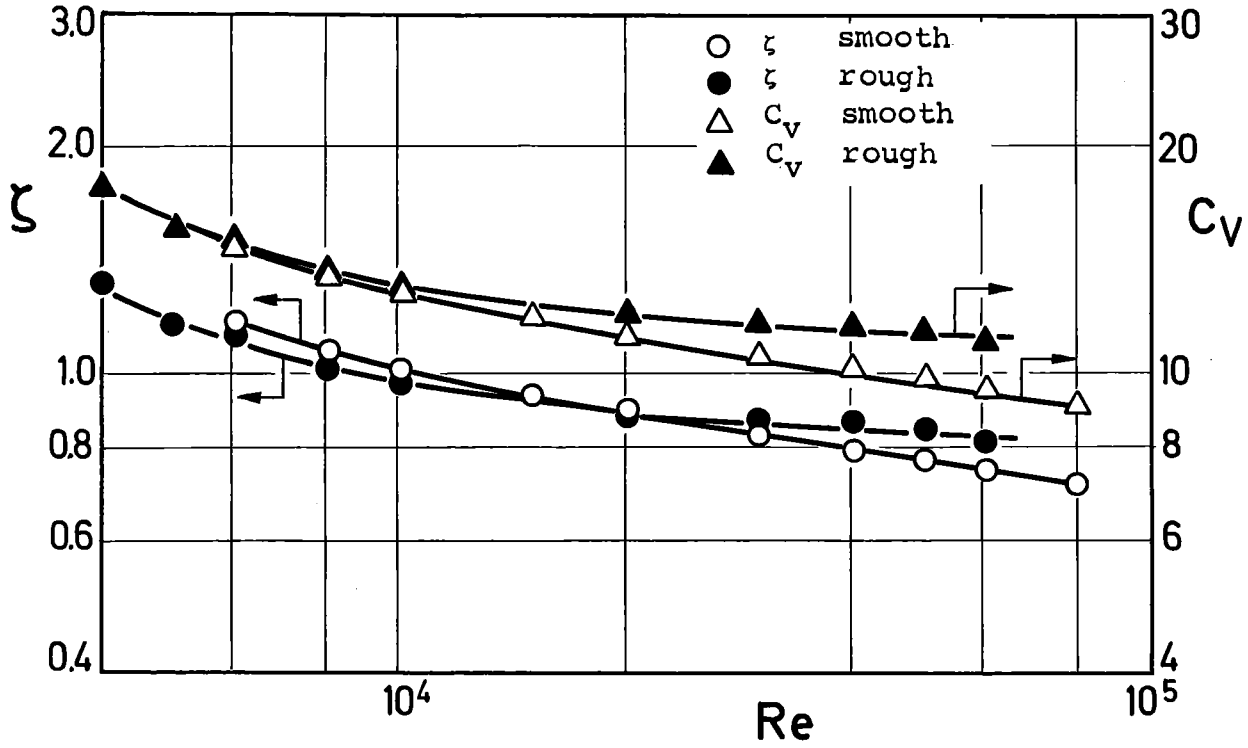

Fig.11: Drag coefficients and modified loss coefficients versus Reynolds number (SIIIS)

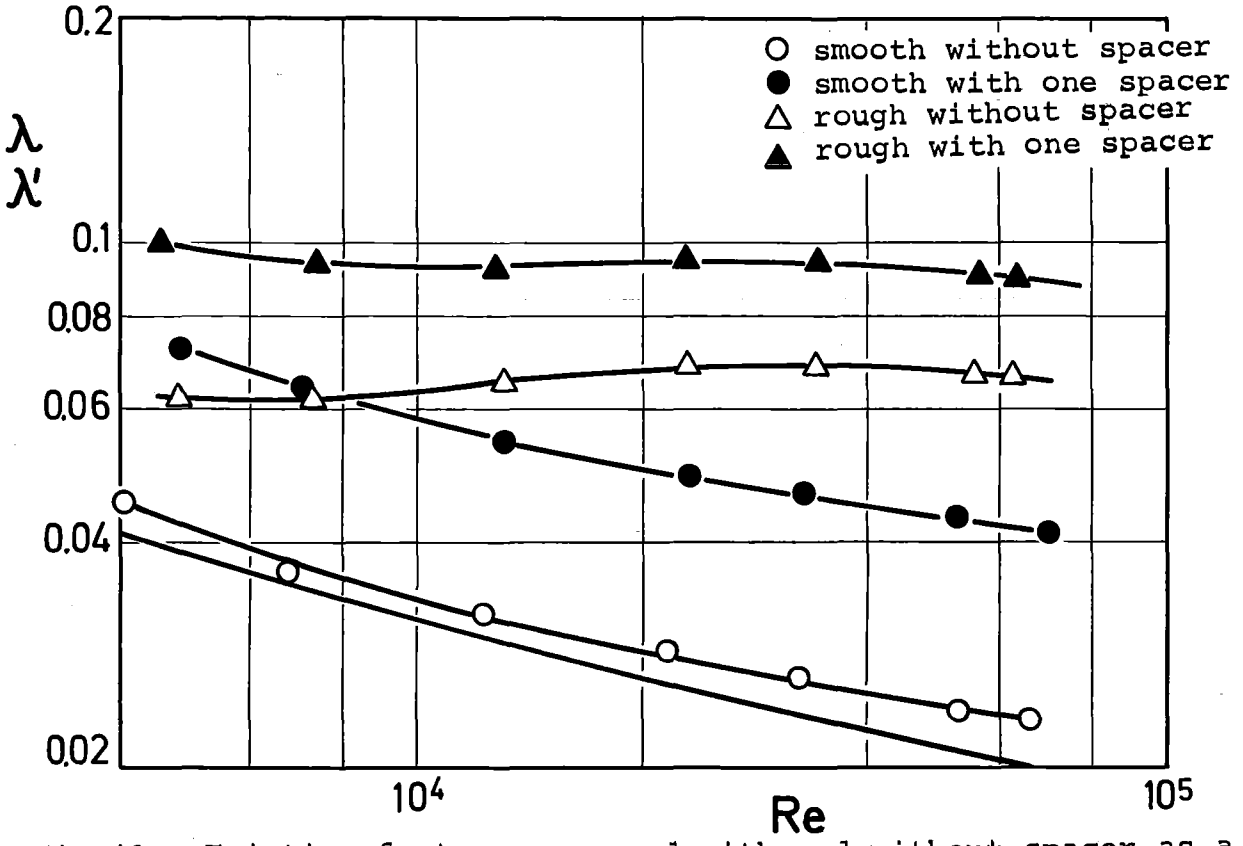

Fig.12: Friction factors measured with and without spacer as a function of the Reynolds number (SIIIR)

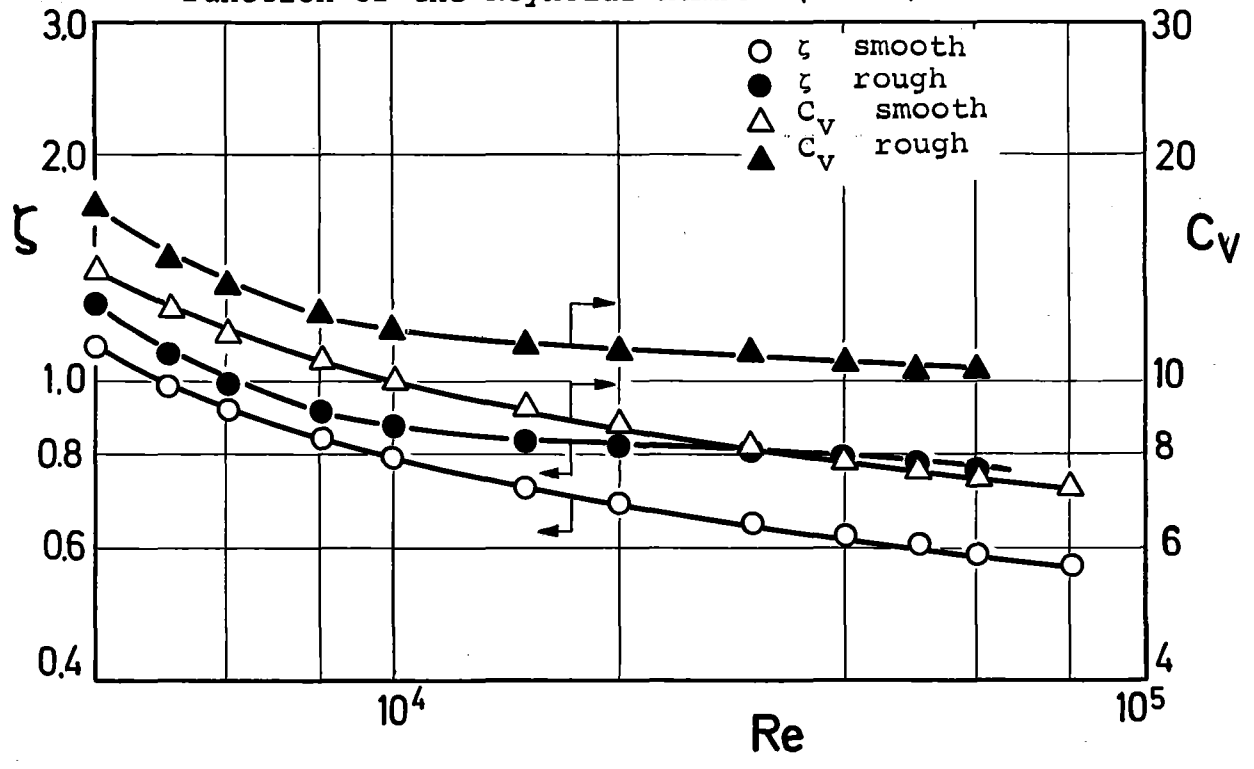

Fig.13: Drag coefficients and modified loss coefficients versus Reynolds number (SIIIR)

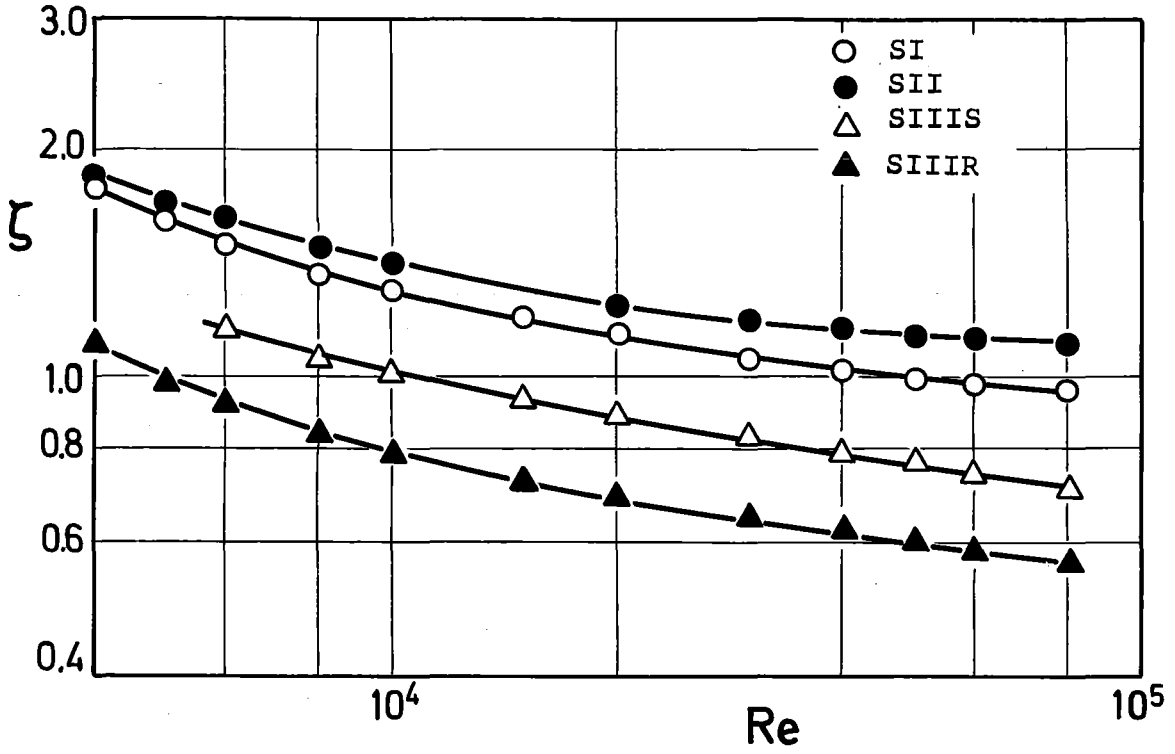

Fig.14: Drag coefficients of the different types of spacer grids in a smooth rod bundle

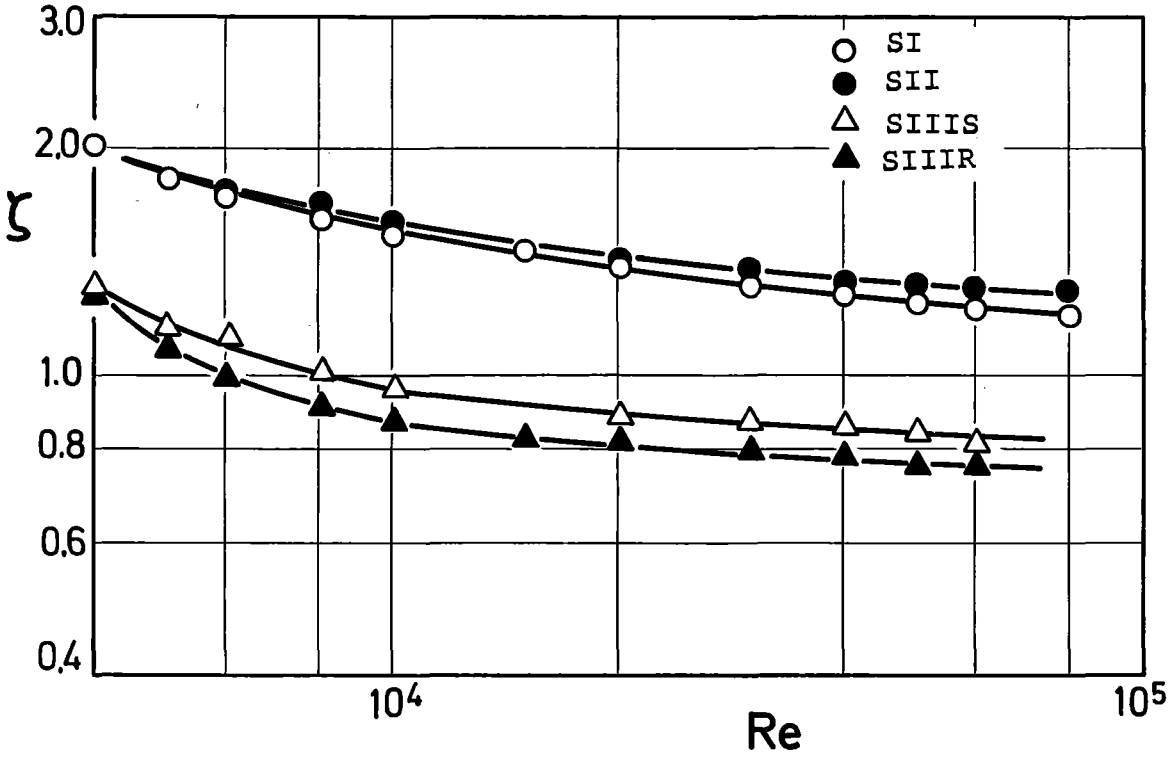

Fig.15: Drag coefficients of the different types of spacer grids in a roughened rod bundle